# High-Precision Measurement of Internuclear Distances using Solid-State NMR

JAE-SEUNG LEE, ANATOLY K. KHITRIN

*Department of Chemistry, Kent State University, Kent, OH 44242-0001*

**ABSTRACT:** Today, nuclear magnetic resonance (NMR) is among the most efficient tools in structural studies. Measurement of interatomic distances is the most common way of determining high-resolution structures of molecules using NMR techniques. In this article, we describe NMR techniques for static powder samples, based on a two-dimensional single-echo scheme, enhanced with adiabatic cross-polarization. They can significantly increase the accuracy of measuring internuclear distances and turn NMR into a high-precision crystallographic technique, complementing the X-ray, and neutron-scattering methods. Experimental examples are presented for intramolecular C—N and C—C distances in α-crystalline form of glycine. © 2008 Wiley Periodicals, Inc. Concepts Magn Reson Part A 32A: 56–67, 2008.

**KEY WORDS:** heteronuclei; adiabatic cross-polarization; dipolar coupling; static solid; internuclear distance

## INTRODUCTION

Nuclear magnetic resonance (NMR) is one of the three major tools, with X-ray and neutron scattering, for studying structures of molecules, crystals, and disordered solids. Traditionally, NMR is used for amorphous or microcrystalline solids, liquid or liquid-crystalline samples, insoluble molecules (like membrane proteins), i.e., in the cases when good crystals are not available or too expensive. Because of lower accuracy, as compared to the X-ray and neutron scattering for single crystals, NMR data are frequently used to generate models that can be further improved by computer simulations. As a result, many NMR structures are not unique. An increased accuracy in measuring internuclear distances would not only expand the traditional applications and eliminate the structural uncertainties, but will also turn NMR into a true high-resolution technique with numerous applications in chemistry, materials science, and structural biology (*1*). In this article, we will show that with modern NMR spectrometers, measuring NMR distances with a relative accuracy better than 0.1% is a realistic task.

Received 1 June 2007; revised 16 August 2007; accepted 20 August 2007

Correspondence to: Jae-Seung Lee; E-mail: jlee2@kent.edu

Concepts in Magnetic Resonance Part A, Vol. 32A(1) 56–67 (2008)

Published online in Wiley InterScience (www.interscience.wiley.com). DOI 10.1002/cmr.a.20101

In NMR, information about internuclear distances is retrieved from the magnitudes of long-range dipole–dipole interactions. For a pair of heteronuclei, the Hamiltonian can be written as

$$H = \omega_I I_z + \omega_S S_z + [\omega_d(1 - 3\cos^2\theta) + J] I_z S_z,$$
$$\omega_d = \frac{\mu_0}{4\pi}\frac{\gamma_I \gamma_S \hbar}{r^3}, \qquad [1]$$

where $\omega_I$ ($\omega_S$) and $\gamma_I$ ($\gamma_S$) are the chemical shift and the gyromagnetic ratio of spin $I$ ($S$) respectively, $\mu_0$ is the permeability of free space, $r$ is the distance between spins $I$ and $S$, $\theta$ is the angle between the external magnetic field and the internuclear vector connecting spins $I$ and $S$, and $J$ is the isotropic spin–spin coupling constant. At this moment, we will neglect the $J$-coupling for simplicity. Each of the spins splits the spectrum of its neighbor into a doublet with the peaks separation $\omega_d(1 - 3\cos^2\theta)$. Therefore, $\omega_d$ in Eq. [1] is the splitting when the internuclear vector is perpendicular to the magnetic field ($\theta = \pi/2$).

Long-range dipole–dipole interactions couple each spin pair to other spin pairs in the sample. This interaction broadens the spectrum of an individual pair. The broadening is proportional to the concentration of spin pairs. Therefore, spin pairs should be made well isolated by lowering their concentration. For well isolated spin pairs with known orientation (single crystal), the accuracy of measuring this splitting and, therefore, the internuclear distance would be limited only by a natural linewidth resulting from spin-lattice relaxation, which can be negligibly small in many solids. Under real experimental conditions, there are other contributions to the line width. The methods of eliminating or reducing them are the major subject for the present article.

Of course, it is desirable to be able to measure internuclear distances in powder samples. It would not only greatly expand the range of possible applications, but will also eliminate the uncertainty coming from a nonperfect crystal orientation. The ideal dipolar line shape for a static powdered sample (*2*) can be derived as follows. The intensity of the spectrum in the interval ($\omega$, $\omega + d\omega$) is contributed by the fraction of a sample in which the internuclear vector is in the interval ($\theta$, $\theta + d\theta$):

$$I(\omega)d\omega \propto \sin\theta d\theta \quad \text{or} \quad I(\omega) \propto \sin\theta(d\omega/d\theta)^{-1}. \qquad [2]$$

By inserting $\omega = \omega_d\,(1 - 3\cos^2\theta)$ and solving with respect to $\omega$, one gets

$$I(\omega) \propto \frac{1}{\sqrt{1 \pm 2\omega/\omega_d}}. \qquad [3]$$

The two mirrored subspectra in Eq. [3] are superimposed in the resulting Pake powder spectrum shown in Fig. 1. The distance between the singularities in this spectrum determines the coupling constant $\omega_d$.

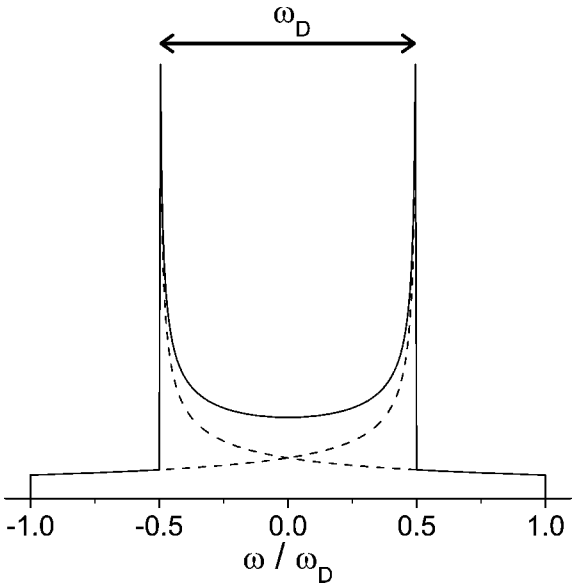


**Figure 1** The ideal dipolar powder spectrum.

However, one can easily see a weak point of this approach. It is a sensitivity problem. The spectral intensity is spread over a broad powder pattern, while it is required that the concentration of spin pairs remains small. Low sensitivity of NMR spectrometers greatly limited a use of the Pake powder patterns, and many other less direct NMR techniques for obtaining information about dipolar couplings have been developed.

SLF (separated-local-field) spectroscopy (*3*), PISEMA (polarization inversion spin exchange at magic angle) (*4*, *5*), as well as more recent techniques: HIMSELF (heteronuclear isotropic mixing leading to spin exchange via the local field) (*6*), PITANSEMA (polarization inversion time averaged nutation spin exchange at the magic angle) (*7*), or SAMMY (magic sandwiches) (*8*) have been used to measure distances between rare and abundant nuclei in oriented samples and single crystals when information about orientation is known. Higher efficiency of heteronuclear decoupling, compared to homonuclear, suggests that better accuracy can be achieved for well-isolated pairs of rare nuclei when the abundant nuclei (protons) are decoupled. A significant number of techniques in solid-state NMR use magic-angle spinning (MAS) of a sample. MAS eliminate the chemical shift anisotropy in powder samples and produces narrow spectral peaks. It also averages the

dipole–dipole couplings, and they could be reintroduced by using a rotational resonance (*9*). Rotor-synchronized recoupling sequences (*10–13*) make it possible to combine sites assignment with information about dipolar couplings. TEDOR (transferred echo double resonance) (*14*) combines information about distances with peaks assignment. When the problem of peaks assignment is not an issue, the most popular techniques for measuring internuclear distances under MAS are rotational echo double resonance (REDOR) (*15*) (for heteronuclear pairs) and its more recent modifications (*16–22*), or build-up of the double-quantum coherence (*23*, *24*) (for homonuclear pairs). For retrieving information about internuclear distances, the experimental spin dynamics under MAS is compared to the results of computer simulation. The simulation usually requires additional information about chemical shift tensors and their orientations with respect to the internuclear vector.

For static samples, the nutation spectroscopy (*25*) or the Carr-Purcell sequence (*26*) (for homonuclear systems), and MLEV-8 sequence with composite pulses (*27*) (for heteronuclear systems) have been used. The effective Hamiltonians, which govern spin dynamics in such experiments, are known only approximately. To solve this problem, in (*26*) the experimental data were extrapolated to infinite intervals between pulses in a Carr-Purcell sequence. Such extrapolation for homonuclear systems is, however, not safe. The frequency of dipolar oscillations of a two-spin system depends on a difference of chemical shifts. Therefore, for a homonuclear spin pair, the dipolar splitting depends not only on the angle between the internuclear vector and the static field but also on orientation of the tensor, which is a difference between the chemical shift tensors for two nuclei. For the same orientation of the internuclear vector, say perpendicular to the magnetic field, different orientations of crystals, allowed by rotations around this internuclear vector, create a distribution of the chemical shift differences and distort the "singular" powder peaks. For heteronuclear systems, the extrapolation to infinite intervals between pulses can be used. However, one would expect better accuracy when the actual, not extrapolated, values are measured.

As we show below, revitalizing the old idea of using the Pake powder patterns today, when the advanced instrumentation and techniques for enhancing sensitivity and resolution are available, may lead to unprecedented accuracy in measuring the NMR distances.

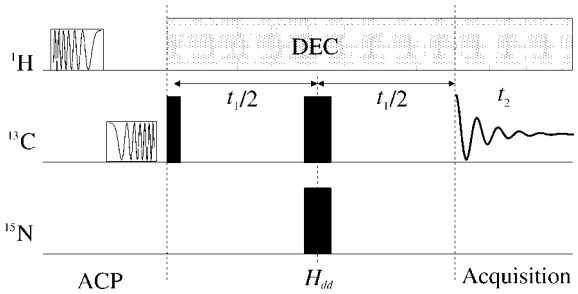


**Figure 2** Experimental pulse sequence consists of adiabatic cross-polarization, evolution ($t_1$), and acquisition ($t_2$) periods.

## THE SINGLE-ECHO METHOD

### The Pulse Sequence

In the single-echo experiment (*28*) the perturbation of the system is physically reduced to minimum, and most of the time the spin system evolves under the unperturbed Hamiltonian (Eq. [1]). A single pair of simultaneous 180° pulses on both of the heteronuclei refocuses the chemical shift interactions. The sensitivity enhancement is achieved by using adiabatic cross-polarization (ACP) (*29*) and efficient heteronuclear decoupling (*30–34*).

The experimental scheme is shown in Fig. 2. Its central part is the spin–echo double-resonance (SEDOR) (*35*) pulse sequence. In a 2D form, this sequence has been used in heteronuclear J spectroscopy (*36*, *37*) and to measure $^{13}$C—$^{15}$N dipolar couplings in a single crystal (*38*). Our scheme starts with ACP to boost polarization of the $^{13}$C nuclei (*29*). Then, $^1$H spins are decoupled, and a 90° pulse creates transverse magnetization of $^{13}$C spins. The $^{13}$C—$^{15}$N spin pair evolves under the dipole–dipole interaction. Two simultaneous 180° pulses on both spins in the middle of the evolution period $t_1$ refocus dephasing by chemical shifts and form an echo at the end of the evolution period. The $^{13}$C NMR signal is acquired in a two-dimensional way by varying the evolution time. The Fourier-transform with respect to the evolution time $t_1$ gives the $^{13}$C—$^{15}$N dipolar powder spectrum.

### Adiabatic Cross-Polarization

Adiabatic cross-polarization (ACP) is an essential element to increase sensitivity and make it possible acquiring the spectra at low concentration of spin pairs. Line broadening from homonuclear dipole–dipole interactions between spins belonging to different pairs is directly proportional to the concentration

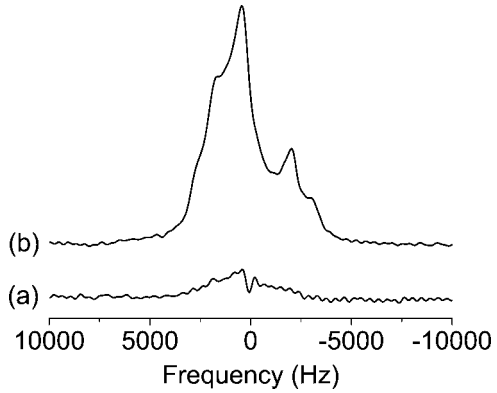


**Figure 3** $^{13}C$ NMR spectrum of 2% glycine-[$^{13}C_\alpha$,$^{15}N$] in glycine: (a) thermal equilibrium spectrum; (b) the spectrum enhanced with adiabatic cross-polarization.

of the spin pairs. Therefore, it is desirable to decrease the concentration of the pairs to the level of $^{13}C$ natural abundance (n. a.) (for $^{13}C—^{15}N$ pairs), or even below if isotopically depleted matrix is used. ACP consists of adiabatic demagnetization/remagnetization in the laboratory frame (ADLF/ARLF), performed with two frequency-sweeping pulses.

The frequency-sweeping pulses are shaped pulses with constant RF amplitude and time-dependent phase. The phase modulation is programmed as $f \times \tau_p \times \pi\,[2(t/\tau_p) - (t/\tau_p)^2]$, where $f$ is the frequency in Hz, $\tau_p$ is the duration of the frequency-sweeping pulse in s, and $0 < t < \tau_p$. With this phase modulation, the pulse changes its frequency linearly with time from $f$ Hz to 0 Hz. The actual frequency at 0 Hz is the transmitter frequency, set by the spectrometer. The efficiency of ACP is illustrated in Fig. 3, showing about seven-fold increase of the $^{13}C$ polarization in glycine. The $^{1}H$ adiabatic pulse had 100 ms duration, 100 kHz frequency-sweeping range, and 1.2 kHz amplitude ($\gamma B_1/2\pi$); the $^{13}C$ pulse had 100 ms duration, 60 kHz frequency-sweeping range and 9.5 kHz amplitude. The amplitudes and the sweeping ranges of the pulses have been optimized experimentally for higher $^{13}C$ polarization. The repetition time has been chosen long enough (25 s) to make the results independent of this time. Of course, in practice one would use much shorter repetition time, comparable to $T_1$ of protons, which is usually considerably less than $^{13}C$ relaxation times. For optimized repetition rate (1 s), the $^{13}C$ polarization enhancement may reach about 30 times for the glycine samples.

## Experimental Results

α-crystalline form of glycine has been previously studied with NMR (*39*, *27*), X-ray (*40*), and neutron scattering (*41–43*). Therefore, it is a good test case to check the performance of various schemes. Isotopically labeled glycine-[$^{13}C_\alpha$,$^{15}N$] (ISOTEC) and glycine-[$^{13}C'$,$^{15}N$] (Aldrich) have been used for measuring short and long $^{13}C—^{15}N$ distances, respectively. Each of the two labeled samples was diluted to 2% in n. a. glycine (Aldrich) and to 1% in isotopically depleted glycine-[$^{12}C_2$,$^{14}N$] (ISOTEC). SPINAL-32 heteronuclear decoupling sequence (*31*) was used to decouple protons.

Figure 4 shows the dipolar powder spectra obtained for the four samples by using the pulse sequence in Fig. 2. Both the "singular" peaks contributed by the internuclear vectors perpendicular to the magnetic field $\left(\theta \approx \frac{\pi}{2}\right)$ and step-like boundaries from the parallel orientation $(\theta \approx 0)$ are clearly seen in the dipolar powder spectra. The central peaks originate from $^{13}C$ spins of the matrix and due to nonperfect 180° pulses.

## Detection by a Low-γ Nucleus ($^{15}N$)

When the sensitivity permits, it is beneficial to use a $^{15}N$ nucleus for detection. Lower $\gamma$ results in decreased broadening factors, and lower $^{15}N$ natural abundance reduces homonuclear broadening from the n. a. spins of the matrix. The dipolar powder spectra for the same four glycine samples as in the previous section, acquired with the $^{15}N$ detection, are shown in Fig. 5. Compared to the spectra in Fig. 4, one can see a significant decrease in the line width. Quite expectedly, the signal-to-noise ratio also drops substantially.

## $^{15}N$ Single-Labeled Sample

Instead of using a doubly $^{13}C$, $^{15}N$-labeled sample one can try only $^{15}N$ labeling and using pairs formed by $^{15}N$ label and $^{13}C$ at natural abundance, when the later happens to occupy a nearby site. This may allow measuring several distances simultaneously. Figure 6 shows 2D $^{13}C$ NMR spectrum for glycine-$^{15}N$ acquired with the pulse sequence in Fig. 2. Because of a large difference in isotropic chemical shifts between $^{13}C_\alpha$ and $^{13}C'$, the dipolar powder spectra for $^{13}C_\alpha—^{15}N$ and $^{13}C'—^{15}N$ pairs are clearly separated. Although the peaks are significantly broadened, as a result of large concentration of $^{15}N$, one can still process this spectrum, by using a simple procedure described later, and obtain quite accurate values for the two intramolecular $^{13}C—^{15}N$ distances in glycine.

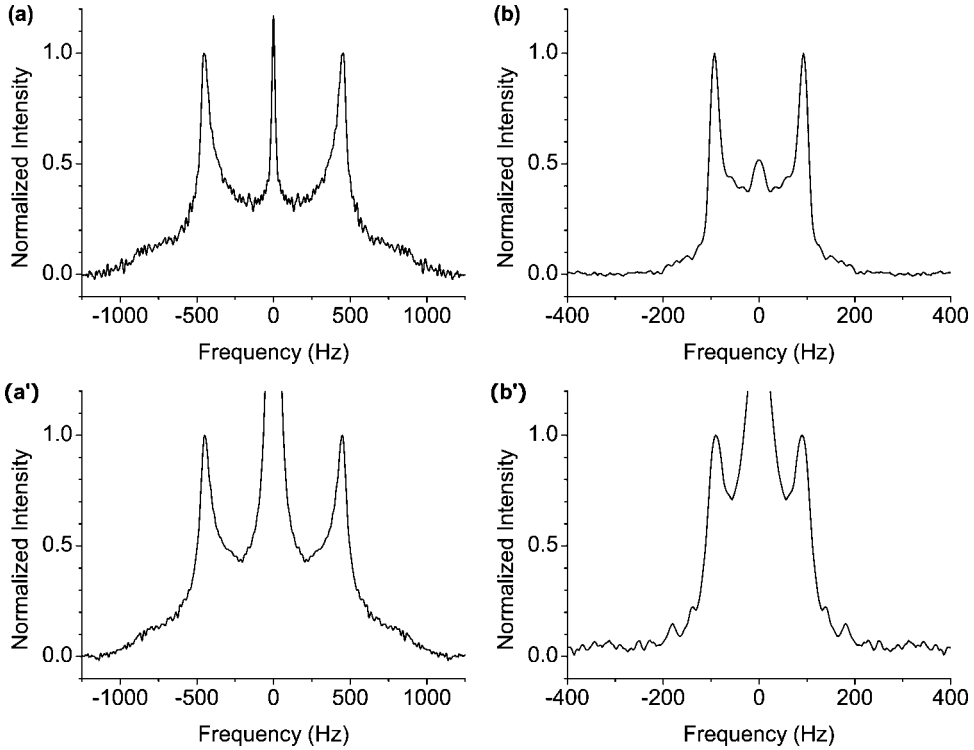


**Figure 4** Dipolar spectra for (a) 1% glycine-[$^{13}C_{\alpha}$,$^{15}N$] in glycine-[$^{12}C_2$,$^{14}N$] (exp. time $\sim$ 16.5 h); (a′) 2% glycine-[$^{13}C_{\alpha}$,$^{15}N$] in glycine (exp. time $\sim$ 20.5 h); (b) 1% glycine-[$^{13}C'$,$^{15}N$] in glycine-[$^{12}C_2$,$^{14}N$] (exp. time $\sim$ 20.5 h); (b′) 2% glycine-[$^{13}C'$,$^{15}N$] in glycine (exp. time $\sim$ 20.5 h).

## Homonuclear Pair ($^{13}C—^{13}C$)

It is interesting to find out if a pulse sequence similar to that in Fig. 2 (without $^{15}N$ pulse) can be used to retrieve information about the $^{13}C—^{13}C$ distance. The spin Hamiltonian for a homonuclear pair is

$$H = \omega_I I_z + \omega_S S_z + \left[\frac{3}{2}\omega_d\left(1 - 3\cos^2\theta\right)\right] I_z S_z + \left[-\frac{1}{2}\omega_d\left(1 - 3\cos^2\theta\right) + J\right]\overrightarrow{I} \bullet \overrightarrow{S}, \qquad [4]$$

where $\omega_d$ is the same as in the Eq. [1]. As it was mentioned in the Introduction, there is a complication for homonuclear pairs because of the dependency of the dipolar splitting on the difference of the chemical shifts. The splitting is given by $\omega_d(1 - 3\cos^2\theta)$ when the difference in chemical shifts is much larger than the dipolar coupling, and increases by 50% when the difference in chemical shifts disappears. This may spoil the singular feature of a dipolar powder pattern and make it difficult evaluating the dipolar coupling constant. Surprisingly, the experimental 2D spectrum for 1% glycine-$^{13}C_2$ in glycine, shown in Fig. 7, produces very sharp "singular" peaks for all traces. Besides that, the peak-to-peak distance is the same for all traces.

Since the shape of the spectrum significantly deviates from the ideal powder pattern (the peaks are more "symmetric") and, at present, there is no good method for data processing, we have tried estimating the internuclear distance under the assumption that the system is heteronuclear. By using the peak-to-peak frequency interval and the literature value $J = 53.1$ Hz (*39*) we estimated the $^{13}C—^{13}C$ distance to be 0.155 nm, which compares well with 0.153 nm from the X-ray experiment (*41*). Such "heteronuclear" treatment of the spectra is expected to work even better for longer $^{13}C—^{13}C$ distances. Of course, if the chemical shift tensors are exactly the same for the two carbons (including the orientation of the tensors), the value $(3/2)\omega_d$ instead of $\omega_d$ should be used in calculations.

## THE CONSTANT-TIME MODIFICATION

The major factor limiting an accuracy of NMR distance measurements is the line broadening, resulting from nonperfect protons decoupling and homonuclear dipole–dipole interactions. A radical method

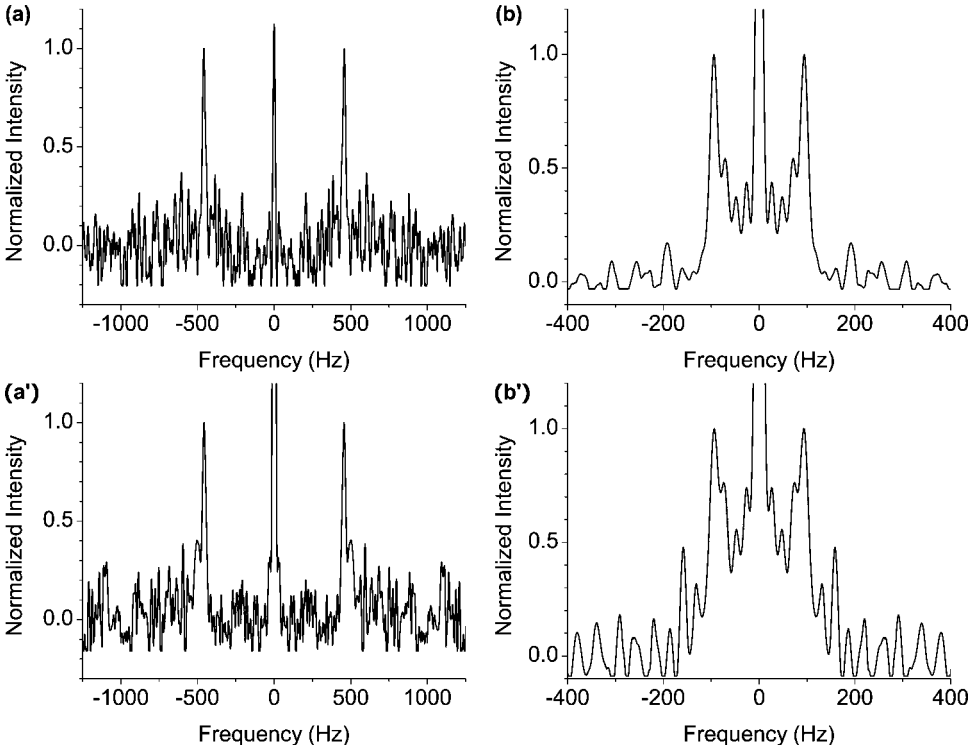


**Figure 5** Dipolar powder spectra obtained with $^{15}N$ detection: (a) 1% glycine-[$^{13}C_\alpha$,$^{15}N$] in glycine-[$^{12}C_2$,$^{14}N$] (exp. time $\sim$ 80 h); (a′) 2% glycine-[$^{13}C_\alpha$,$^{15}N$] in glycine (exp. time $\sim$ 47 h); (b) 1% glycine-[$^{13}C'$,$^{15}N$] in glycine-[$^{12}C_2$,$^{14}N$] (exp. time $\sim$ 90 h); (b′) 2% glycine-[$^{13}C'$,$^{15}N$] in glycine (exp. time $\sim$ 40 h).

of eliminating the line broadening for directly detected nuclei is using the constant-time (*44*) measurement. Of course, better resolution is reached at a cost of decreased sensitivity. The proposed experimental scheme (*45*) is shown in Fig. 8.

The scheme works as follows. The first "sliding" 180° pulse at $t_1/2$ ($t_1 < \tau$, where $\tau$ is the echo time) changes the sign of the heteronuclear dipole–dipole coupling and reverses the evolution. The second 180° pulse for another nucleus, applied at $\tau/2$, restores the sign of the dipolar coupling. Therefore, at the echo time $\tau$ the net evolution "in one direction" will correspond to the evolution time $t_1$.

The dipolar powder spectrum for 2% glycine-[$^{13}C_\alpha$,$^{15}N$] in glycine, obtained with $^{13}C$ detection and constant echo time of 25 ms, is shown in Fig. 9. Compared to the experiment with variable echo time for the same sample [Fig. 4(a′)] the line broadening decreased from 59 Hz to 24 Hz.

The result for a longer C—N distance is shown in Fig. 10 for 2% glycine-[$^{13}C'$,$^{15}N$] in glycine. With the constant-time scheme, the Lorentzian broadening factor has decreased from 26 Hz to 12 Hz. The estimated $^{13}C$—$^{15}N$ NMR distance, 0.253 nm, is consistent with the one determined in (*28*).

Another advantage of the constant-time scheme is a possibility to significantly decrease the central peak from the matrix by using a standard dc correction in 2D Fourier transform of the Varian VNMRJ software. This is valuable since in many cases the use of isotopically depleted matrices may be cost-prohibited.

## DATA PROCESSING

From the Pake powder patterns, the information about internuclear distances can be retrieved by using a very simple data processing. The details of the procedure can be found in (*28*). Here we will briefly describe the main steps.

The three major factors that need to be taken into account are: 1) line broadening, which comes from nonperfect proton decoupling and homonuclear interactions; 2) scalar *J*-coupling for the case of the nearest neighbors; and 3) the delayed acquisition in $t_1$ dimension.

### Line Broadening

The signal decays with increasing the evolution time $t_1$. This line broadening shifts the "singular" peaks at $\pm\omega_d/2$ toward the center of the spectrum. For

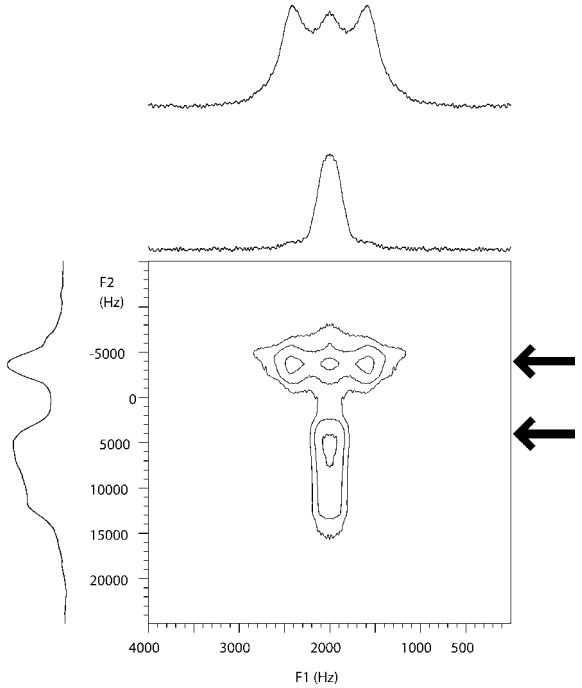


**Figure 6** 2D $^{13}C$ NMR spectrum for glycine-$^{15}N$ obtained with the pulse sequence in Fig. 2 (exp. time $\sim$ 44 h). Two traces shown above are taken at the frequency positions indicated by the arrows.

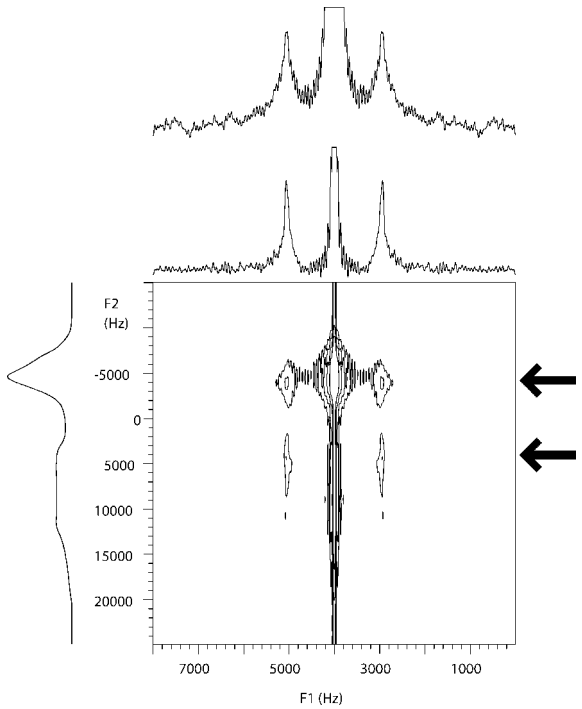


**Figure 7** 2D $^{13}C$ NMR spectrum for 1% glycine-$^{13}C_2$ in glycine (exp. time $\sim$ 42 h). Two traces shown above are taken at the frequency positions indicated by the arrows.

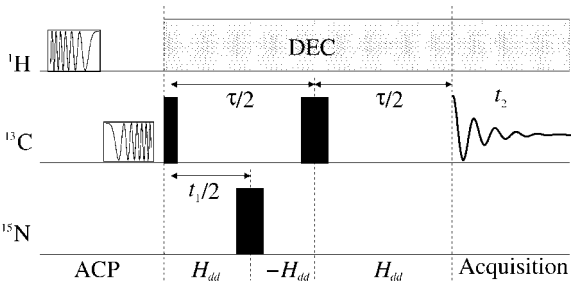


**Figure 8** The scheme with constant echo time for measuring heteronuclear coupling constants.

Lorentzian broadening (exponential decay of the signal), the simulated theoretical spectra for three different broadening factors are shown in Fig. 11. Even though the peak positions shift toward the center of the spectrum at increasing broadening factor, all the spectra cross the frequency $\pm\omega_d/2$ at the same relative height, about 90% of the maximum. Therefore, the correction can be made by simply measuring the spectral interval between the two outside points at 90% of relative intensity.

## *J*-Coupling

For the directly bonded nuclei, the scalar *J*-coupling should be taken into account. Although the value of *J*-coupling can be obtained from fitting the spectra, like in Fig. 4(a), the values measured in a solution may often provide a sufficient accuracy and save from introducing an extra fitting parameter.

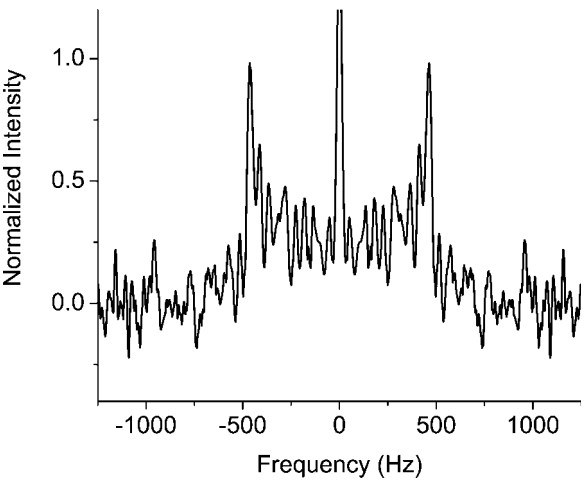


**Figure 9** Dipolar spectrum for 2% glycine-[$^{13}C_\alpha$,$^{15}N$] in glycine (exp. time $\sim$ 75 h, $\tau$ = 25.0 ms), recorded with the constant-time pulse sequence in Fig. 8.

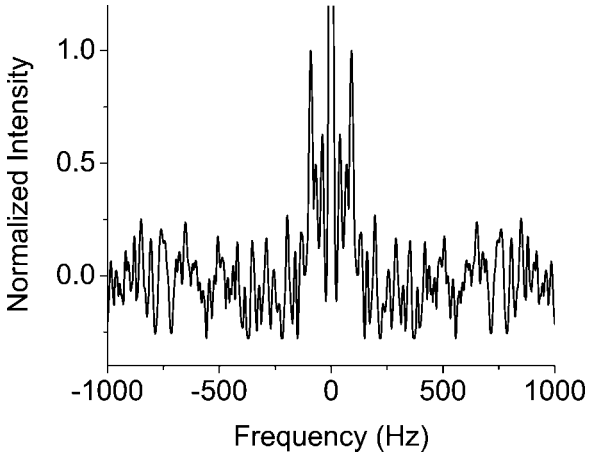


**Figure 10** The dipolar powder spectrum obtained with the constant-time experiment for 2% glycine-[$^{13}C'$,$^{15}N$] in glycine (exp. time ~89 h, $\tau$ = 32.0 ms).

### Acquisition Delay

The distortion from the 180° pulses is small but not zero. Finite duration of the pulses and after-pulse delays create an acquisition delay $\tau_a$ in the $t_1$ dimension. In the absence of line broadening, the acquisition delay affects the shape of the spectrum but does not shift the positions of the singular peaks. Interference between line broadening and acquisition delay produces a frequency shift described by the following empirical formula:

$$\frac{\Delta\omega}{2\pi} = 2.2 \times \frac{\omega_d}{2\pi} \times (4 \times \Delta f) \times \tau_a, \qquad [5]$$

where $\Delta f$ is the distance in frequency between the points of 90% and 70% intensities on the outside slope of a "singular" peak. The Lorentzian broadening factor is $4\Delta f$.

The step-by-step calculations for four glycine samples are shown in Table 1. For the neighbor $^{13}C$ and $^{15}N$ the value $J$ = 6.7 Hz, measured separately in a solution, has been used. The signs of $J$-coupling and the dipolar coupling at $\theta = \pi/2$ are the same (negative). Therefore, 6.7 Hz was subtracted from the frequency interval between the points at 90% height. This correction is relatively small if one compares it to the overall error bars of 5 Hz for the coupling constant. After obtaining the corrected values of $\omega_d$ the internuclear distances $r_{NMR}$ are calculated as

$$r_{NMR} = \left(\frac{\mu_0}{4\pi}\frac{\gamma_1\gamma_S\hbar}{\omega_d}\right)^{1/3}. \qquad [6]$$

A comparison of the spectrum in Fig. 4(a) with the theoretical one is presented in Fig. 12. In the theoretical spectrum, the experimental value of the acquisition delay $\tau_a$ = 100 μs, which is a sum of the $^{15}N$ pulse duration (80 μs) and two after-pulse delays (10 μs each), has been used. Deviations between the theoretical and experimental spectra are due to the fact that the line-broadening factor depends on crystals orientation and, as a result, the total spectrum cannot be fitted using a uniform line broadening. This is one of the reasons why we are using narrow spectral regions of the outside slopes of the "singular" peaks for retrieving information about dipolar coupling constants, rather than trying to extract this information from fitting the total powder pattern.

## ATOMIC VIBRATIONS

The dipolar-coupling constant $\omega_d$ measured by NMR is a quantity averaged over molecular motions. Modulation of the distance $r$ between nuclei and the angle $\theta$ affects the measured $\omega_d$ and, therefore, the calculated distance $r_{NMR}$. We can mention here the works (*46*, *47*) where the role of molecular librations has been studied. When $r_{NMR}$ is determined from positions of the "singular" peaks in the powder spectrum $\left(\theta \approx \frac{\pi}{2}\right)$ it is convenient to consider the deviations $r = r_0 + \Delta$, $|\Delta| \ll r_0$, and $\theta \equiv \frac{\pi}{2} - \delta$, $|\delta| \ll 1$. Then, the effect of atomic vibrations on $r_{NMR}$ can be estimated as (*28*)

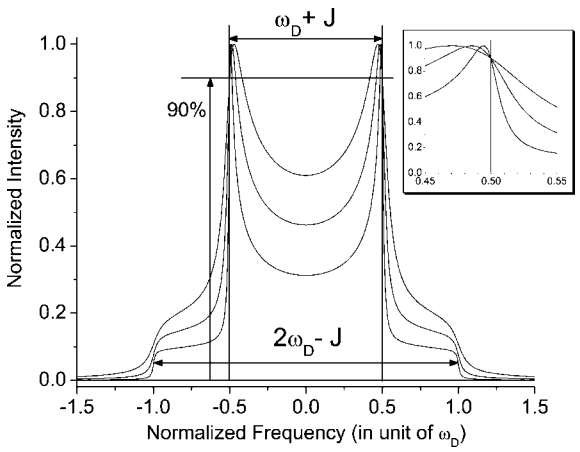


**Figure 11** Simulated spectra for different relative broadening factors: 2, 5, and 10%. Although the peak positions shift with increasing broadening factor, the spectral intervals between the points at 90% of relative peak intensity can be consistently measured, as shown in the inset.

**Table 1 Experimental Results for Intramolecular $^{13}C—^{15}N$ Distances in α-Glycine**

| Sample | $(\omega'_d + J)/2\pi$ (Hz) | $4 \times \Delta f$ (Hz) | $\omega_d/2\pi$ (Hz) | $r_{NMR}$ (Å) |
|---|---|---|---|---|
| 1% glycine-[$^{13}C_\alpha$,$^{15}N$] in glycine-[$^{12}C_2$,$^{14}N$] | 929.21 (924.64) | 35.9 (14.8) | 915.21 (914.29) | 1.4959 (1.4964) |
| 2% glycine-[$^{13}C_\alpha$,$^{15}N$] in glycine | 925.67 (923.40) | 59.4 (17.9) | 906.97 (912.28) | 1.5004 (1.4975) |
| 1% glycine-[$^{13}C'$,$^{15}N$] in glycine-[$^{12}C_2$,$^{14}N$] | 195.62 (196.07) | 15.9 (13.4) | 194.94 (195.36) | 2.5048 (2.5029) |
| 2% glycine-[$^{13}C'$,$^{15}N$] in glycine | 197.80 (196.22) | 25.8 (15.5) | 196.68 (195.40) | 2.4973 (2.5028) |

$(\omega'_d + J)/2\pi$ is the frequency interval at 90% height, $4 \times \Delta f$ is the measured line-broadening factor, and $\omega_d/2\pi$ is the dipolar coupling constant after correction for the acquisition delay. The data in parentheses are obtained with $^{15}N$ detection.

$$r_{NMR} \equiv \left(\frac{\gamma_1\gamma_S\hbar}{\omega_d}\right)^{1/3} \approx r_0\left(1 - 2\frac{\langle\Delta^2\rangle}{r_0^2} + \langle\delta^2\rangle\right), \quad [7]$$

where $r_0$ is the equilibrium distance between nuclei. Alternatively, the equilibrium distance $r_0$ can be calculated from $r_{NMR}$:

$$r_0 \approx r_{NMR}\left(1 - \langle\delta^2\rangle\right) + \frac{2\langle\Delta^2\rangle}{r_{NMR}} \quad [8]$$

when the variances of Δ and δ are known. At room temperature, $C_\alpha$—N stretching is mainly contributed by zero-point vibration. $\langle\Delta^2\rangle = 2.378 \times 10^{-3}$ Å$^2$ (*28*) is small and produces only 0.3% decrease of $r_{NMR}$ compared to $r_0$. $\langle\delta^2\rangle$, which increases $r_{NMR}$ compared to $r_0$, may have contributions from many low-frequency thermally-excited modes. According to the molecular dynamics simulation (*46*) the average variance of the Euler angles for molecular librations of the $C_\alpha$—N bond in glycine is $\langle\delta^2\rangle = 0.01273$ rad$^2$. It would make $r_{NMR}$ longer than $r_0$ by about 1% or 0.02 Å. This estimate of the difference between $r_{NMR}$ and $r_0$ is comparable to the differences between the results obtained with NMR and other techniques (Table 2).

## FUTURE IMPROVEMENTS

There are no fundamental limitations for further increase of the accuracy in NMR distance measurements. Potentially, it can be so high that the data might be used for refining structures obtained with X-ray and neutron scattering. In this section, we will try to envision several future developments of the described technique.

### Increasing Sensitivity: Hardware

As one could see from the previous discussion, enhanced sensitivity can be directly converted into higher accuracy of measuring the coupling constants. Better signal-to-noise (S/N) ratio decreases uncertainties of the data processing, allows using lower concentration of the pairs to make homonuclear broadening negligible, and/or longer echo times in the constant-time experiment. Any of the conventional approaches to increasing S/N (*48*), or their combinations, will be helpful. They may include customized probes with better sensitivity and higher proton decoupling power, higher-field magnets, cryoprobes, and cold amplifiers.

### Heteronuclear Decoupling

The quality of proton decoupling was the major factor limiting resolution in the presented experimental examples. The constant-time method described earlier reduces the line broadening at a cost of the reduced signal. In practice, the constant echo time can be made only a few times longer than the echo decay time. Therefore, quality heteronuclear decoupling is necessary to increase resolution (by increasing

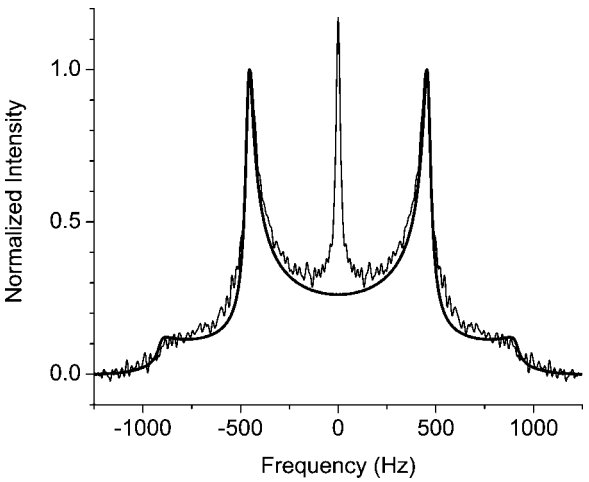


**Figure 12** Comparison of experimental (thin line) and theoretical (thick line) powder spectra for 1% glycine-[$^{13}C_\alpha$,$^{15}N$] in isotopically depleted glycine-[$^{12}C_2$,$^{14}N$].

**Table 2 Comparison of Experimental Results for $C_\alpha$—N Distance in α-Glycine**

| | | |
|---|---|---|
| Solid state NMR | Our result, 1% glycine-[$^{13}C_\alpha$,$^{15}N$] in isotopically depleted glycine-[$^{12}C_2$,$^{14}N$]. | 1.496 ± 0.002 Å |
| | NMR, $^{13}C$—$^{15}N$, ref. (*20*, *35*) 10% glycine-[$^{13}C_\alpha$,$^{15}N$] in glycine | 1.505 (−0.001, 0.002) Å |
| | NMR, $^{13}C$—$^{14}N$, single crystal, ref. (*29*) 9% glycine-$^{13}C_2$ in glycine | 1.509 ± 0.009 Å |
| X-ray and neutron | Neutron scattering I, ref. (*31*) | 1.476 ± 0.001 Å |
| | Neutron scattering II, ref. (*32*) | 1.475 ± 0.001 Å |
| | X-ray diffraction, ref. (*30*) | 1.474 ± 0.005 Å |

the echo time) and/or decrease the experimental time. The SPINAL decoupling sequence (*31*) is especially efficient for static samples. However, as explained in (*32*, *33*), there exist no universal "ultimate" decoupling sequence. The choice of the decoupling scheme would depend on the available decoupling power and the sample. The constant-time scheme also brings some specifics to the decoupling problem. In each particular case, one may try searching for a more efficient decoupling scheme, by using a strategy described in (*33*).

## Adiabatic Cross-Polarization

The seven-fold $^{13}C$ signal enhancement shown in Fig. 3 is still very far from the theoretical maximum. The frequency-sweeping pulses used for ACP have not been optimized yet. Possible ways of improving the efficiency of ACP are mentioned in (*29*). Better shapes of the frequency-sweeping pulses are expected to provide larger signal enhancement. Recently, we have found that simultaneous frequency-sweeping pulses have slightly better performance.

## Temperature-Dependent Measurements

X-ray scattering senses an electronic density, distorted by chemical bonds, and, therefore, provides only indirect information about positions of the nuclei. Neutron scattering has its own limitations, including low sensitivity. Today, the most accurate results are achieved by combining the data from the X-ray and neutron-scattering experiments. NMR may become the third high-precision crystallographic technique, used in combination with X-ray and neutron scattering. However, molecular vibrations affect differently the results of different methods, and more work on quantifying the vibrational contributions is needed before different techniques can complement each other. A convenient comparison point for all techniques is the equilibrium distance at zero temperature. A contribution to NMR distance from the zero-point quantum vibrations is relatively small, and can be estimated easier than the contribution from thermal atomic vibrations. Today, an accuracy of NMR distance measurement is already sufficient for obtaining reliable temperature dependence and extrapolating it to zero temperature.

## Cryogenic Measurements

A more straightforward solution would be eliminating the thermal vibrations experimentally by performing the experiment at the liquid-helium temperature of the sample. $T_1$ relaxation time can be reduced by paramagnetic doping and made suitable for the 2D experiment. Protons can be repolarized by paramagnetic centers via spin-diffusion, and ACP to rare spins will be even more efficient at longer relaxation times. At low temperature, there also exists an exciting opportunity to use a dynamic nuclear polarization (DNP) (*49*). DNP in a high-field magnet (700 MHz proton frequency) has been recently realized (*50*).

## Other Heteronuclear Pairs

Of course, the method is not limited to $^{13}C$—$^{15}N$ pairs. It can be applied in exactly the same way to the other spin ½ nuclei: $^{1}H$, $^{19}F$, $^{29}Si$, $^{31}P$, $^{77}Se$, $^{111,113}Cd$, $^{115,117,119}Sn$, etc., if well isolated pairs of heteronuclei are present or created in a sample. As convenient spin-1/2 pairs, one can use, as an example, the pairs $^{13}C$—$^{19}F$, $^{13}C$—$^{31}P$, or $^{29}Si$—$^{1}H$. The constant-time scheme in Fig. 8 allows using a partial echo, because the unchangeable part of the signal is subtracted by the data processing. Therefore, it will be possible to have a quadrupolar nucleus like $^{2}H$ or even $^{14}N$ as an "indirect" nucleus of the pair. Pairs with deuterium are especially interesting since the X-ray scattering does not provide accurate data on the hydrogen's locations.

## CONCLUSION

Greatly increased sensitivity of modern NMR spectrometers, combined with efficient heteronuclear decoupling and cross-polarization techniques, opens

new ways to using the Pake powder patterns for measuring internuclear distances in solids. 2D NMR experiments, producing unperturbed dipolar powder spectra, can be done for spin pairs diluted to 1% or even lower concentration. This may turn NMR into a high-precision crystallographic tool, complementing the X-ray, and neutron-scattering methods. The increased accuracy of internuclear distance measurements will also expand the traditional applications of NMR to resolving structures of amorphous, disordered, or micro-crystalline solids.

## REFERENCES


1. Ramamoorthy A, ed. 2006. NMR Spectroscopy of Biological Solids. Boca Raton; CRC/Taylor & Francis.
2. Pake GE. 1948. Nuclear resonance absorption in hydrated crystals: fine structure of the proton line. J Chem Phys 16:327–336.
3. Waugh JS. 1976. Uncoupling of local field spectra in nuclear magnetic-resonance-determination of atomic positions in solids. Proc Natl Acad Sci USA 73: 1394–1397.
4. Wu CH, Ramamoorthy A, Opella SJ. 1994. High-resolution heteronuclear dipolar solid-state NMR-spectroscopy. J Magn Reson A 109:270–272.
5. Ramamoorthy A, Wei Y, Lee DK. 2004. PISEMA solid-state NMR spectroscopy. Annu Rep NMR Spectrosc 52:1–52.
6. Dvinskikh SV, Yamamoto K, Ramamoorthy A. 2006. Heteronuclear isotropic mixing separated local field NMR spectroscopy. J Chem Phys 125:034507.
7. Lee DK, Narasimhaswamy T, Ramamoorthy A. 2004. PITANSEMA, a low-power PISEMA solid-state NMR experiment. Chem Phys Lett 399:359–362.
8. Nevzorov AA, Opella SJ. 2007. Selective averaging for high-resolution solid-state NMR spectroscopy of aligned samples. J Magn Reson 185:59–70.
9. Raleigh DP, Levitt MH, Griffin RG. 1988. Rotational resonance in solid-state NMR. Chem Phys Lett 146: 71–76.
10. Fujiwara T, Ramamoorthy A, Nagayama K, Hioka K, Fujito T. 1993. Dipolar HOHAHA under MAS condition for solid-state NMR. Chem Phys Lett 212:81–84.
11. Fujiwara T, Khandelwal P, Akutsu H. 2000. Compound radiofrequency-driven recoupling pulse sequences for efficient magnetization transfer by homonuclear dipolar interaction under magic-angle spinning conditions. J Magn Reson 145:73–83.
12. Kristiansen PE, Carravetta M, van Beek JD, Lai WC, Levitt MH. 2006. Theory and applications of supercycled symmetry-based recoupling sequences in solid-state nuclear magnetic resonance. J Chem Phys 124:234510.
13. Dusold S, Sebald A. 2000. Dipolar recoupling under magic-angle spinning conditions. Annu Rep NMR Spectrosc 41:185–264.
14. Jaroniec CP, MacPhee CE, Bajaj VS, McMahon MT, Dobson CM, Griffin RG. 2004. High-resolution molecular structure of a peptide in an amyloid fibril determined by magic angle spinning NMR spectroscopy. Proc Natl Acad Sci USA 101:711–716.
15. Gullion T, Schaefer J. 1989. Rotational-echo double-resonance NMR. J Magn Reson 81:196–200.
16. Garbow JR, Gullion T. 1992. The importance of precise timing in pulsed, rotor-synchronous MAS NMR. Chem Phys Lett 192:71–76.
17. Hughes E, Gullion T. 2004. A simple, inexpensive, and precise magic angle spinning speed controller. Solid State Nucl Magn Reson 26:16–21.
18. Fu RQ, Smith SA, Bodenhausen G. 1997. Recoupling of heteronuclear dipolar interactions in solid state magic-angle spinning NMR by simultaneous frequency and amplitude modulation. Chem Phys Lett 272:361–369.
19. Gullion T, Pennington CH. 1998. θ-REDOR: an MAS NMR method to simplify multiple coupled heteronuclear spin systems. Chem Phys Lett 290:88–93.
20. Chan JCC, Eckert H. 2001. C-rotational echo double resonance: heteronuclear dipolar recoupling with homonuclear dipolar decoupling. J Chem Phys 115: 6095–6105.
21. Schmidt-Rohr K, Hong M. 2003. Measurements of carbon to amideproton distances by C–H dipolar recoupling with N-15 NMR detection. J Am Chem Soc 125:5648–5649.
22. Gan ZH. 2006. Rotary resonance echo double resonance for measuring heteronuclear dipolar coupling under MAS. J Magn Reson 183:235–241.
23. Carravetta M, Edén M, Johannessen OG, Luthman H, Verdegem PJE, Lugtenburg J, et al. 2001. Estimation of carbon–carbon bond lengths and medium-range internuclear distances by solid-state nuclear magnetic resonance. J Am Chem Soc 123:10628–10638.
24. Carravetta M, Zhao X, Johannessen OG, Lai WC, Verhoeven MA, Bovee-Geurts PHM, et al. 2004. Protein-induced bonding perturbation of the rhodopsin chromophore detected by double-quantum solid-state NMR. J Am Chem Soc 126:3948–3953.
25. Yannoni CS, Kendrick RD. 1981. NMR nutation spectroscopy–a method for determining molecular-geometry in amorphous solids. J Chem Phys 74:747–749.
26. Engelsberg M, Yannoni CS. 1990. The determination of bond lengths in solids using the Carr-Purcell sequence. J Magn Reson 88:393–400.
27. Ishii Y, Terao T. 1995. Determination of interheteronuclear distances by observation of the pake-doublet patterns using the MLEV-8 sequences with composite pulses. J Magn Reson A 115:116–118.
28. Lee JS, Khitrin AK. 2006. Accurate measurement of $^{13}C$-$^{15}N$ distances with solid-state NMR. J Chem Phys 124:144508.
29. Lee JS, Khitrin AK. 2005. Adiabatic cross-polarization via intermediate dipolar-ordered state. J Magn Reson 177:152–154.

30. Bennett AE, Rienstra CM, Auger M, Lakshmi KV, Griffin RG. 1995. Heteronuclear decoupling in rotating solids. J Chem Phys 103:6951–6958.
31. Fung BM, Khitrin AK, Ermolaev K. 2000. An improved broadband decoupling sequence for liquid crystals and solids. J Magn Reson 142:97–101.
32. Khitrin A, Fung BM. 2000. Design of heteronuclear decoupling sequences for solids. J Chem Phys 112: 2392–2398.
33. Khitrin AK, Fujiwara T, Akutsu H. 2003. Phase-modulated heteronuclear decoupling in NMR of solids. J Magn Reson 162:46–53.
34. De Paëpe G, Eléna B, Emsley L. 2004. Characterization of heteronuclear decoupling through proton spin dynamics in solid-state nuclear magnetic resonance spectroscopy. J Chem Phys 121:3165–3180.
35. Slichter CP. 1996. Principles of Magnetic Resonance. Berlin: Springer; 311 p.
36. Freeman R, Hill HDW. 1971. High-resolution study of NMR spin echoes: "J-spectra." J Chem Phys 54: 301–313.
37. Freeman R. 1998. Spin Choreography. Oxford: Oxford University Press.
38. Schneider DM, Tycko R, Opella SJ. 1987. High-resolution solid-state triple nuclear magnetic resonance measurement of $^{13}C$-$^{15}N$ dipole-dipole couplings. J Magn Reson 73:568–573.
39. Haberkorn RA, Stark RE, Willigen H, Griffin RG. 1981. Determination of bond distances and bond angles by solid-state nuclear magnetic resonance–$^{13}C$ and $^{14}N$ NMR study of glycine. J Am Chem Soc 103:2534–2539.
40. Marsh RE. 1958. A refinement of the crystal structure of glycine. Acta Cryst 11:654–663.
41. Jönsson PG, Kvick Å. 1972. Precision neutron diffraction structure determination of protein and nucleic acid components. III. The crystal and molecular structure of the amino acid α-glycine. Acta Cryst B 28:1827–1833.
42. Power LF, Turner KE, Moore FH. 1976. The crystal and molecular structure of α-glycine by neutron diffraction—a comparison. Acta Cryst B 32:11–16.
43. Thaper CL, Dasannacharya BA, Goyal PS, Chakravarthy R, Tomkinson J. 1991. Neutron-scattering from glycine and deuterated glycine. Physica B 174:251–256.
44. Bax A, Freeman R. 1981. Investigation of complex networks of spin–spin coupling by two-dimensional NMR. J Magn Reson 44:542–561.
45. Lee JS, Khitrin AK. 2007. Constant-time method for measuring inter-nuclear distances in static powders. J Magn Reson 186:327–329.
46. Ishii Y, Terao T, Hayashi S. 1997. Theory and simulation of vibrational effects on structural measurements by solid-state nuclear magnetic resonance. J Chem Phys 107:2760–2774.
47. Hallock KJ, Lee DK, Ramamoorthy A. 2000. The effects of librations on the 13C chemical shift and 2H electric field gradient tensors in b-calcium formate. J Chem Phys 113:11187–11193.
48. Fujiwara T, Ramamoorthy A. 2006. How far the sensitivity of NMR experiments can be increased? Ann Pep NMR Spectrosc 58:155–175.
49. Abragam A, Goldman M. 1982. Nuclear Magnetism: Order and Disorder. Oxford: Clarendon Press.
50. Hornstein MK, Bajaj VS, Griffin RG, Kreischer KE, Mastovsky I, Shapiro MA, et al. 2005. Second harmonic operation at 460 GHz and broadband continuous frequency tuning of a gyrotron oscillator. IEEE Trans Elec Dev 52:798–807.

## BIOGRAPHIES

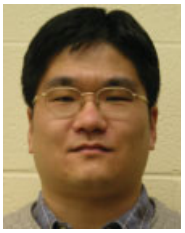

**Jae-Seung Lee** received his Ph.D. in physics from the Korea Advanced Institute of Science and Technology in 2003 under the guidance of Professor Soonchil Lee. Since 2003, he has been working as a research fellow in the Department of Chemistry at the Kent State University. His research interests include developing NMR techniques and NMR-based quantum information processing.

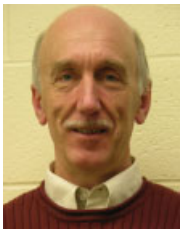

**Anatoly K. Khitrin** graduated from Moscow Institute of Physics and Technology in 1978. After that, he worked in the Institute of Chemical Physics in Chernogolovka, Russia, with Boris Provotorov. In 1999 he moved to the University of Oklahoma. Since 2002, Dr. Khitrin is an associate professor at Kent State University in USA. His major research interests are spin dynamics and NMR.